New Journal of Physics
The open access journal at the forefront of physics

Deutsche Physikalische Gesellschaft DPG
IOP Institute of Physics

Published in partnership with: Deutsche Physikalische Gesellschaft and the Institute of Physics

OPEN ACCESS

RECEIVED
11 August 2018

REVISED
10 October 2018

ACCEPTED FOR PUBLICATION
17 October 2018

PUBLISHED
6 November 2018

Original content from this work may be used under the terms of the Creative Commons Attribution 3.0 licence.

Any further distribution of this work must maintain attribution to the author(s) and the title of the work, journal citation and DOI.

PAPER

Exactly solvable dynamics of forced polymer loops

Wenwen Huang[1], **Yen Ting Lin**[1,2], **Daniela Frömberg**[1], **Jaeoh Shin**[1], **Frank Jülicher**[1] and **Vasily Zaburdaev**[1,3,4]

[1] Max Planck Institute for the Physics of Complex Systems, Nöthnitzer Str. 38, D-01187 Dresden, Germany
[2] Theoretical Division and Center for Nonlinear Studies, Los Alamos National Laboratory, New Mexico 87545, United States of America
[3] Friedrich-Alexander Universität Erlangen-Nürnberg, Cauerstr. 11, D-91058 Erlangen, Germany
[4] Author to whom any correspondence should be addressed.

E-mail: wenwen@pks.mpg.de **and** vzaburd@pks.mpg.de

Keywords: Bethe ansatz, ASEP, polymer loop

Abstract

Here, we show that a problem of forced polymer loops can be mapped to an asymmetric simple exclusion process with reflecting boundary conditions. The dynamics of the particle system can be solved exactly using the Bethe ansatz. We thus can fully describe the relaxation dynamics of forced polymer loops. In the steady state, the conformation of the loop can be approximated by a combination of Fermi–Dirac and Brownian bridge statistics, while the exact solution is found by using the fermion integer partition theory. With the theoretical framework presented here we establish a link between the physics of polymers and statistics of many-particle systems opening new paths of exploration in both research fields. Our result can be applied to the dynamics of the biopolymers which form closed loops. One such example is the active pulling of chromosomal loops during meiosis in yeast cells which helps to align chromosomes for recombination in the viscous environment of the cell nucleus.

1. Introduction

Simple models in polymer physics capture generic polymer features [1, 2]. These features are often very robust and govern behaviors of experimentally observed systems. For example, the freely jointed chain model [2] can capture the statistics of spatial configurations of a polymer and explain its behavior in situations where the free energy is dominated by configurational entropy [2, 3].

The problem of polymer dynamics raises additional challenges. The Rouse model, representing a polymer as a chain of beads connected by harmonic springs [4], its extension to account for hydrodynamic interactions between the beads by Zimm [5], and the reptation model [1] were successful in describing various aspects of polymer dynamics, relaxation and rheology [1, 2]. In experimentally relevant settings, polymers are often subjected to geometrical constraints such as confinement, pinning, or looping [6–9]. Further level of complexity exists in a biological context when the systems of interest are intrinsically out of equilibrium and thus the applicability of the concepts from equilibrium statistical physics is limited. Therefore, the situations where models of polymer dynamics can be solved exactly are rare but exist. In this paper, we present an exact solution for the dynamics of the forced polymer loop. This solution is based on an unexpected mapping of the polymer problem to a well known many-particle dynamical system: the asymmetric simple exclusion process (ASEP).

We demonstrate that the one-dimensional version of the forced pinned polymer loop model can be mapped to the ASEP model with reflecting boundaries. We obtain exact solution to the dynamics of the ASEP model [10–12] by using the Bethe ansatz method. In particular, this allows us to calculate the longest relaxation time of the polymer loop as a function of the external force. Interestingly, the relaxation time calculated for the one-dimensional model provides an excellent estimation for the longest relaxation time of a three-dimensional polymer chain in the direction of the force obtained in Brownian dynamics simulations. In the steady state regime, we find that the conformations of the one-dimensional polymer are well approximated by a combination of Fermi–Dirac and Brownian bridge statistics. They are exactly enumerated via the fermion

© 2018 The Author(s). Published by IOP Publishing Ltd on behalf of Deutsche Physikalische Gesellschaft

integer partition theory. Thus the central result of this paper is the full analytical description of both the stationary state and dynamics of the forced polymer loop via the mapping to the exactly solvable ASEP model.

Loop geometry is generically occurring both in polymer and biological problems [13–22]. Recently, we have shown that the model of forced polymer loops could be used to quantify homologous chromosome alignment in yeast cells [23]. During meiosis in fission yeast, chromosomes in the nucleus form loops and are actively pulled by molecular motors from one end of the elongated cell to the other in a periodic movement [24, 25]. In this process, viscous drag forces stretch the chromosomal loops, which reduces configurational fluctuations and brings the chromosomes in physical proximity, suitable for recombination. By considering the period of the movement when chromosomes are pulled with nearly constant speed, this non-equilibrium problem could be mapped to the equilibrium fluctuations of a three-dimenensional pinned and forced polymer loop in an external force field. The statistics of the steady state configuration of the loop could be obtained from a theory of random walks and the partition function approach [23]. However, this analysis only provided predictions for the stationary state and left the dynamics of the process beyond its reach. The theory developed in this study fully covers the *dynamics* of the pinned and forced polymer loops.

The manuscript is organized as follows. In section 2 we motivate the setting of the pinned and forced polymer loops. We begin with a brief introduction to a three-dimensional model and then formulate the corresponding one-dimensional version. All analytical results in this paper are for this one-dimensional model. We will return to three-dimensions in the final parts of the paper when comparing the analytical results to the Brownian dynamics simulations. In section 3, we map the configurations and dynamics of the one-dimensional polymer loop model to those of the particle system. In section 4, we provide the solution to the stationary regime both by an approximate Brownian bridge theory and by the exact integer number partition theory. In section 5, we solve the dynamics of the ASEP model and illustrate how the exact solution of the one-dimensional system can be used to describe the relaxation dynamics of the three-dimensional polymer loop in section 6. Finally, discussion and conclusions can be found in section 7.

2. Pinned and forced polymer loops

We consider the statistics of static configurations and the dynamics of polymers that form closed loops and that are pulled by an external field while being pinned at one point. An interesting example for such a system is given by the movement of chromosomes in fission yeast during meiosis. Three pairs of homologous chromosomes of the fission yeast bind their telomeric ends to a single protein complex thus forming a loop configuration. Microtubles protruding from this protein complex in the cytoplasm are being pulled on by molecular motors. Molecular motor activity and micrtotubule polymerization/depolymerization dynamics result in a periodic movement of the chromosomes and the whole nucleus inside of the elongated cell [24]. The role of this periodic motion is the alignment of chromosomes that is necessary for recombination to happen. During half of the period of nuclear movement, chromosomal loops are pulled with nearly constant speed [24] through the viscous intracellular environment. The viscous drag force stretches the chromosomal loops and thus helps them to align for recombination. Microscopic scales of the problem, low velocity of motion and high viscosity of the intracellular environment correspond to the regime of low Reynolds numbers.

We therefore consider a setting of the polymer loop pulled with a constant speed through a viscous fluid, see figure 1(a). By changing the coordinate system to the frame of references moving with the pulling speed, we obtain the situation where a polymer loop is pinned at the pulling point and stretched by the viscous forces due to the constant velocity motion of the surrounding fluid. If we neglect the forces arising from the hydrodynamic self-interaction of the polymer we arrive at a simplified picture, where a uniform Stokesian drag force F acts on every monomer of the loop, figure 1(b). Thus we made a transition from a polymer loop pulled with a constant speed through a viscous fluid (figure 1(a)) to a polymer that is pinned and stretched by a constant force field (figure 1(b)).

We are interested to study fluctuations in such a system of a pulled and pinned polymer loop. If a pinned polymer loop is stretched by an external conservative force field, the system relaxes to a thermodynamic equilibrium and one can apply equilibrium statistical mechanics at fixed temperature T. The dynamic fluctuations and the response functions in such system obey the fluctuation dissipation theorem. In the case where the force field results from hydrodynamic friction forces due to pulling of a polymer loop at constant velocity, as is the case during nuclear movement in yeast cells, the force field is not conservative and the system is not near thermodynamic equilibrium. In this latter case, fluctuations and response do not obey a fluctuation dissipation theorem and equilibrium statistical mechanics does not hold.

In this study, we consider for simplicity the case where Boltzmann statistics can capture static fluctuations and a fluctuation dissipation theorem holds. This case corresponds either rigorously to a pinned and pulled polymer loop in a conservative force field or it serves as an approximation for a pinned polymer loop that is

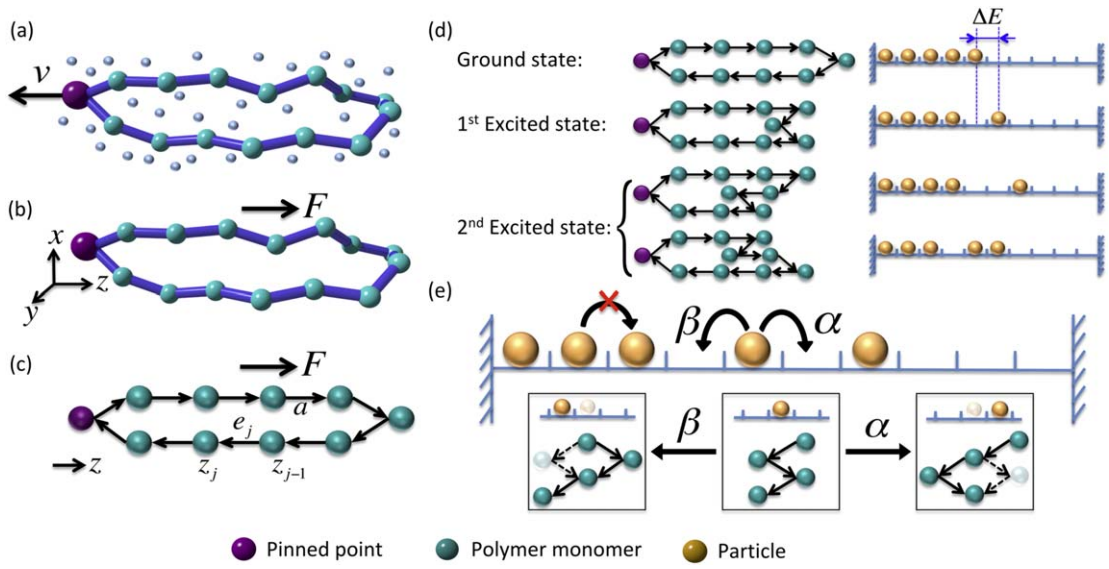

Figure 1. Mapping of a forced pinned polymer loop model to a particle system. (a) Polymer loop pulled with a constant speed through the viscous fluid in three-dimensions. Viscous drag forces stretch the polymer loop. (b) In the co-moving frame of reference, the loop is pinned (magenta colored bead). By neglecting the hydrodynamic self-interaction of the polymer, there is a constant viscous drag force F acting on every monomer in z-direction. (c) Sketch of the one-dimensional polymer loop. Each bead j is characterized by its coordinate z_j. Two beads are separated by a distance a. Each rod connecting two consequent beads $j-1$ and j has an associated direction e_j which can take two values ± 1. External force points in the positive direction of the z-axis. (d) Several possible configurations of a one-dimensional polymer mapped to the configurations of particles on the lattice. In the lattice, the energy of the particle increases from left to right. The energy gap between two neighboring lattice sites is $\Delta E = 2aF$. Flipping of rods against the force field in the polymer model corresponds to a particle configuration with higher energy. (e) The hopping of a particle corresponds to the flipping of two rods connecting to the same bead. Only a pair of two differently directed rods can flip, which corresponds to hopping of a particle to an empty lattice site. Hopping to occupied sites is forbidden. The hopping process is asymmetric as indicated by two different hopping rates α and β. It is energetically more favorable to flip the rod along the force field, than against it.

pulled by hydrodynamic flow. This approximation is very good if fluctuating forces can be well approximated by Gaussian white noise. The system can then be mapped to an equilibrium system and the noise strength plays the role of an effective temperature. The validity of such an approximation has to be tested in an experimental situation such as the chromosome movements in fission yeast [23]. In the following we focus on this equilibrium case and also use it as a simplified model for the non-equilibrium case that provides the main motivation for our work. We now introduce the forced and pinned polymer model and its one-dimensional version.

2.1. Polymer model of the pinned and forced loop

We consider a polymer loop that is pinned at one point and is subjected to a constant force vector **F** acting on every monomer in the polymer chain, see figure 1(b). The polymer is represented as a chain of beads located at positions $\mathbf{r}_i$ with $i = 0, 1, \ldots, L$, freely jointed by rigid rods in three-dimensional space [2]. The rod length a corresponds to the Kuhn length of the polymer and the number of monomers is denoted by L. The polymer is subjected to fluctuations characterized by an effective temperature T. For simplicity, we do not consider excluded volume effects. This three-dimensional model has been used to study the statistics of spatial configurations of the polymer loop in the steady state [23]. In the present work we are interested in the dynamics of this model. We first introduce a one-dimensional version of this model which permits the use of powerful analytic approaches discussed in sections 3–5. We will also use the three-dimensional model to perform Brownian dynamics simulations described in section 6.

2.2. One-dimensional pinned forced polymer loop

In one-dimension, the position of the bead i is denoted by the coordinate z_i, $i = 0, 1, \ldots, L$, see figure 1(c). A constant external force F acts on every bead along the z-coordinate in the positive direction. We characterize the direction of the rod j as $e_j = (z_j - z_{j-1})/a$ which can assume two values $e_j = \pm 1$, either pointing along or against the force. The position of every bead is the sum over all rod directions leading to this bead multiplied by the length of the rod: $z_i = a\sum_{j=1}^{i} e_j$. The loop is pinned at beads $i = 0$ and $i = L$ implying $z_0 = z_L = 0$. The configuration of the loop is uniquely defined by the set of directions of every rod $\{e_i\}_{i=1}^{L}$. Importantly, the setup of the one-dimensional polymer loop can be mapped to a particle system both in its stationary configurations and dynamics.

3. Mapping of a one-dimensional polymer loop to a particle system

We can map the configuration of the one-dimensional polymer model to a one-dimensional many-particle system on a lattice. The two possible directions of every rod $e_j = \pm 1$ are mapped to the state Z_j of a lattice site j, which is either occupied by a particle ($Z_j = 1$) when the rod points along the force or empty ($Z_j = 0$) if the rod points against the force, see figure 1(d). We then have $Z_j = (e_j + 1)/2$ and the positions of the beads are

$$z_i = a\left(2\sum_{j=1}^{i} Z_j - i\right). \tag{1}$$

The loop condition $z_0 = z_L$ imposes a hard constraint of the total number of the particles $\sum_{j=1}^{L} Z_j = L/2$ with a clear physical interpretation: there must be an equal number of rods pointing along and against the force field to form a loop.

3.1. Mapping the polymer configurations

Each polymer loop configuration can be characterized by the corresponding potential energy, which is defined as the work against the external force acting on the beads required to generate a configuration:

$$E = -\sum_{i=1}^{L} F z_i = -Fa\sum_{i=1}^{L}\sum_{j=1}^{i} e_j. \tag{2}$$

By exchanging the order of the double summation in equation (2) and utilizing the loop condition $z_0 = z_L = 0$ we obtain the potential energy in particle representation:

$$E = \tilde{E} + \Delta E\sum_{j=1}^{L} jZ_j, \tag{3}$$

where $\tilde{E} = -L(L+1)\Delta E/4$ and $\Delta E = 2Fa$. One immediately recognizes the similarity between the energy expression equation (3) and the energy of a system consisting of $L/2$ Fermions distributed over L equidistant energy levels $\Delta E, \ldots, L\Delta E$, where Z_j can be interpreted as an occupation number. Clearly the lowest energy of the system corresponds to $Z_j = 1$ for $j \leqslant L/2$ and $Z_j = 0$ otherwise (a fully stretched polymer loop), see figure 1(d). When the system is in contact with a thermal bath at temperature $T > 0$, it is possible to excite other configurations. Importantly, for all energy levels except for the ground state, there are multiple corresponding polymer (or equivalently particle) configurations, see figure 1(d). Thus the task of finding the equilibrium statistics of the system is equivalent to quantifying the degeneracy of each energy level.

3.2. Mapping the polymer dynamics

Configurations of the polymer loop can evolve in time if two rods that connect to the same bead simultaneously flip their orientation (see illustration in figure 1(e)). This process corresponds, in particle representation, to a particle hopping on a lattice. The flip can occur only if the two rods that connect to the bead have opposite directions. In the particle picture, that means there is an empty lattice site next to a particle where it can hop to. A particle cannot hop to a lattice site that is already occupied by another particle. For simplicity, we shall assume that only single-particle hopping is allowed for the rest of our analysis. In the polymer picture, this corresponds to demanding that only the smallest segment of the loop—a single bead—is allowed to move at any given time, and there are no simultaneous movements of longer segments.

The resulting process in the particle picture is a one-dimensional ASEP, see figure 1(e). The pinning condition implies that there is no hopping beyond the boundaries at $i = 0$ and $i = L$, thus the boundaries are reflecting. In the polymer picture, for each flip, one bead has to travel a distance of $\pm 2a$. The asymmetry of the flipping process results from the force acting on the beads: if, as a result of the flip, the bead moves in the direction of the force, such flip will be energetically more favorable than flipping the bead against the force. Thus we see that the dynamics of the one-dimensional polymer loop can be mapped to the ASEP problem. We can now describe this dynamics using the language of the ASEP model [10–12].

We denote the rate of particle hopping to the right and to the left with α and β respectively. In order to map the dynamics, we start with the case $F = 0$. In this case, there is no bias of any configurations so we have $\alpha = \beta$. The value of the hopping rates is related to the flipping time scale of two rods in the polymer picture. Note that in the strictly one-dimensional setting, we cannot define the continuous process of flipping but only its initial and final states. For now we estimate the flipping time by a typical time scale τ_0 for a bead to diffuse a distance of the order of the rod length a in one-dimension. Then the total hopping rate $r := \alpha + \beta$ can be estimated as

$$r = 1/\tau_0 = \frac{2D}{a^2} = \frac{2k_BT}{\gamma a^2}, \tag{4}$$

where we used the diffusion constant of the bead given by Einstein relation $D = k_B T/\gamma$ and γ is the friction coefficient [26]. As a result, we have $\alpha = \beta = r/2$ in the case of $F = 0$. Importantly, later we will be able to validate this hopping rate by benchmarking our results with the Rouse theory (see below).

Now we turn to the case $F \neq 0$. In this case, the hopping of particles is biased by the external force field, and we assume the local detailed balance condition [12, 27] to be fulfilled:

$$\alpha/\beta = \exp(-\Delta E/k_B T), \tag{5}$$

where ΔE is the energy change when flipping a bead against the force field. We emphasize that equation (5) in general does not mean the system is in equilibrium, for which the detailed balance condition $\alpha/\beta = P^{\rm eq}(\eta)/P^{\rm eq}(\eta')$ has to be fulfilled. Here $P^{\rm eq}(\eta)$ is the equilibrium probability of the configurations η and η' which are different by a single hopping step of one particle to the left. ASEP with periodic boundary condition is an example where the local detailed balance holds while the global detailed balance is violated because $P^{\rm eq}(\eta)$ is uniform. However, the global detailed balance is satisfied for the case of reflecting ASEP discussed here [12, 28].

In order to fully determine the hopping rates α and β, one more constraint is required in the case of $F \neq 0$. Here, we adopt the same argument used in driven lattice gas systems [12]. Namely, by introducing an external force field, the hopping rate along the force field β is enhanced by a factor κ so that $\beta = \kappa r/2$, and the hopping rate against the force field α is reduced by the same factor so that $\alpha = \kappa^{-1} r/2$. Then, from equation (5), we can easily obtain $\kappa = \exp(\Delta E/2k_B T)$, and the corresponding left and right-hopping rates for the ASEP system:

$$\alpha = \frac{k_B T}{\gamma a^2} \exp(-\Delta E/2k_B T), \tag{6a}$$

$$\beta = \frac{k_B T}{\gamma a^2} \exp(\Delta E/2k_B T). \tag{6b}$$

The mapping can be generalized to other topologies of the polymer, for example, an unpinned polymer loop corresponds to $L/2$ particles on L lattice sites with periodic boundaries and a free polymer chain corresponds to an open lattice of length L filled by arbitrary (but not larger than L) number of particles. Having described the mapping of the one-dimensional pinned polymer loop model to the ASEP system, we now turn to its detailed analysis starting from the stationary state regime.

4. Stationary state statistics of the polymer loop

There are two approaches to describe the stationary state statistics of the polymer loop: the first one is an approximate solution based on the concept of random walks, and the second one is exact and based on integer number partition theory. We first give the approximate solution via the random walk approach.

4.1. Random walks with Fermi–Dirac statistics

In the absence of force, the configuration of the loop in space is equivalent to a trajectory of a one-dimensional unbiased random walk [29] consisting of L steps, where each step corresponds to a rod in the chain. This random walk, however, has to start and end at the same point to fulfill the loop constraint. Mathematically, this is known as the Brownian bridge problem and can be solved to find the statistics of every bead position to be Gaussian with its variance depending on the index of the bead in the chain [30–32]. We generalize the Brownian bridge solution to the case of non-zero force: we first clarify how the statistics of random walk steps changes in the presence of a force and then we enforce the Brownian bridge condition to form a loop [23].

To find the statistics of the random walks in the presence of the force, we use the mapping to the particle system. The probability to make the ith step along the direction of the force is equivalent to the occupation probability Z_i of the lattice site i. To calculate occupation probabilities, we first relax the fixed number of particles constraint and use the grand canonical ensemble, which allows for the exchange of particles with an external reservoir [33, 34]. We will require the number of particles to be equal to $L/2$ on average, which corresponds to the loop condition being satisfied only on average. We then use the Brownian bridge condition to reinforce the fixed number constrain and thus the exact fulfillment of the loop condition.

In the grand canonical ensemble the probability distribution of Z_j corresponding to energy in equation (3) is the *Fermi–Dirac* distribution [23, 33]:

$$\mathbb{P}\{Z_j = 1\} = \left\{1 + \exp\left[\frac{\Delta E(j-\mu)}{k_B T}\right]\right\}^{-1}, \tag{7a}$$

$$\mathbb{P}\{Z_j = 0\} = 1 - \mathbb{P}\{Z_j = 1\}, \tag{7b}$$

with a chemical potential $\mu = (L+1)/2$ obtained from the requirement that on average there are $L/2$ particles in the system. With relation of Z_j and the direction $e_j = (2Z_j - 1)$ of rod j we can compute the distribution of e_j. The Fermi–Dirac distribution reveals that in the presence of the external force field, the first half of the steps is biased in the direction of force, whereas the second half of steps has higher probability of pointing against the force field. Given the probability distribution of the occupation numbers (and equivalently the directions of the rod), their mean and variance can be easily calculated:

$$\mathbb{E}[Z_j] = \mathbb{P}\{Z_j = 1\}, \tag{8a}$$

$$\mathrm{var}[Z_j] = \mathbb{P}\{Z_j = 1\} \cdot \mathbb{P}\{Z_j = 0\} - (\mathbb{E}[Z_j])^2. \tag{8b}$$

From the statistics of individual steps we can construct the corresponding random walk process. Let us look at its trajectory connecting beads k and l, $l > k$ and the corresponding propagator $\rho(z_l = z|z_k = 0)$. Remarkably, according to the Lindeberg–Feller central limit theorem [35, 36], in the limit $l - k \gg 1$, this propagator is Gaussian with mean and variance equal to the sum of mean and variance of all individual steps leading from bead k to l. We therefore found the statistics of random walks in the presence of the external force field. However, due to the grand canonical approach, such random walks return to the origin only on average. While this random walk correctly describes the mean position of every bead, it does not capture the fluctuations of bead position. To determine the variance of the bead position we have to enforce the loop condition.

4.2. Imposing the loop condition

The Brownian bridge condition ensures that a bead with an index i is a part of a random walk loop of length L. At the bead i two pieces of random walk trajectory with lengths i and $L - i$ meet at the position of the bead and belong to the same loop. Thus the probability density function of finding the bead i at a given coordinate z is given by [23, 32].

$$\rho^L(z_i = z) = \frac{\rho(z_i = z|z_0 = 0)\rho(z_{L-i} = z|z_L = 0)}{\rho(z_L = 0|z_0 = 0)}. \tag{9}$$

In the case of the pinned polymer loop, the propagators in the above expression are Gaussian distributions with a mean and variance obtained as a sum of means and variances of all contributing individual steps of the random walk. Importantly, because each propagator entering the above equation (9) is Gaussian, the resulting $\rho^L(z_i = z)$ is Gaussian as well. It has a variance

$$\mathrm{var}[z_i^L] = \frac{\sum_{j=1}^{i}\mathrm{var}[Z_j]\sum_{j=L-i+1}^{L}\mathrm{var}[Z_j]}{\sum_{j=1}^{L}\mathrm{var}[Z_j]}, \tag{10}$$

where $\mathrm{var}[Z_j]$ is given by (8b). We can now compare these results with direct Monte Carlo simulations of the one-dimensional pinned polymer loop in an external force field (which in practice are the simulations of the corresponding ASEP model). In figure 2, we plot the mean (a) and variance (b) of the positions of the beads for different strengths of the external force field. With increasing force, the polymer becomes more stretched and the fluctuations decrease. In the limit of zero force, we recover the well known result of the standard Brownian bridge problem [35]. Although calculating the sums involved in the estimation of the mean and variance does not present any particular difficulty, for large temperatures the sums can be approximated by integrals and evaluated explicitly (see appendix A for details).

4.3. Fermion integer number partition theory

Although the Brownian bridge approach provides a good estimates of the mean and the variance of the equilibrium position of every bead, it is an approximation relying on the central limit theorem and thus requiring that the number of beads is sufficiently large. Here we derive the exact solution of the stationary state of the ASEP with reflecting boundaries using restrictive integer partition theory [37]. Exact solution of this particular model can be obtained. It establishes links to the number theory and theory of ASEP. First we change the basis of the fermionic many-particle system from its microscopic configurations $\{Z_1, Z_2, \ldots, Z_L\}$ to its total energy, which can only take discrete values E_0, $E_0 + \Delta E$, …, $E_0 + L^2\Delta E/4$, where E_0 is the ground state. In this representation, the configuration space is a one-dimensional lattice with a finite support. Without loss of generality, we set the constant energy $E_0 = 0$. The difficulty of using this basis is to determine the degeneracy of the microscopic states which have the same energy. We denote the number of microscopic states with energy E as $g(E)$. Once $g(E)$ is known, the partition function of the system in the canonical ensemble can be formally written as

$$\mathcal{Z}(T) = \sum_E g(E)\mathrm{e}^{-\frac{E}{k_BT}}, \quad E \in \{0, \Delta E, 2\Delta E, \cdots, L^2\Delta E/4\}. \tag{11}$$

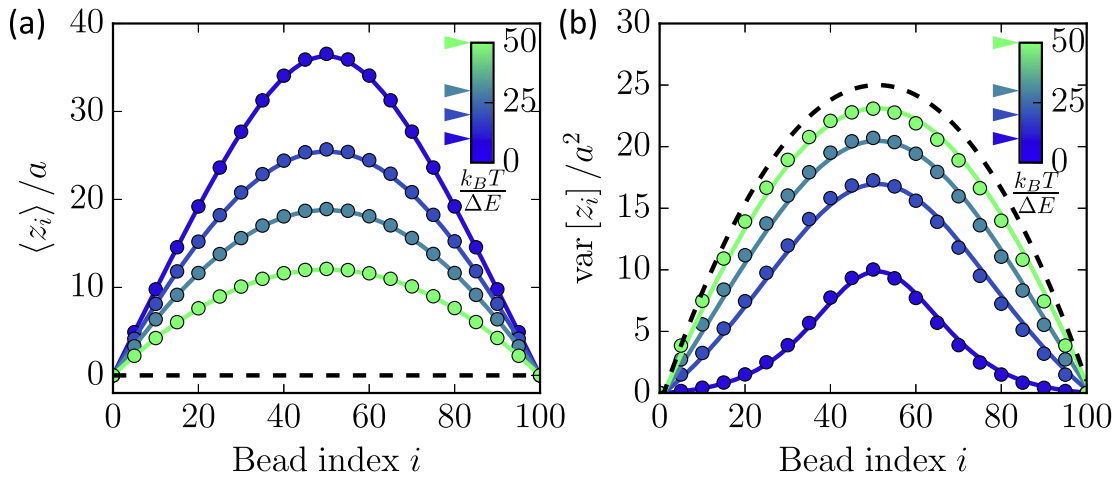

Figure 2. Stationary state statistics of the loop. Mean (a) and variance (b) of the position of beads in the one-dimensional pinned polymer loop from Monte Carlo simulation results (dots) are compared to theoretical results (solid lines). The number of beads in the polymer loop is $L = 100$. The dashed line indicates the case of no external force $k_B T/\Delta E \to \infty$. Other values of $k_B T/\Delta E$ are shown by different colors as indicated in the legend.

The problem of determining $g(E)$ can be solved with the help of the closely related problem of integer partition in number theory [37]. Consider the system with the energy $E = \sum_{n=1}^{L/2} E_n$, where E_n is the energy of the particle n. Then $g(E)$ is the number of possible ways to partition the total energy E into the summation of $L/2$ components E_n with the constraint $0 \leqslant E_1 \leqslant E_2 \cdots \leqslant E_{L/2} \leqslant L\Delta E/2$. Since E_n is discretized by ΔE, $g(E)$ is identical to $g(K)$, which is the number of possible ways to partition the integer K into the summation of $L/2$ integers $K = \sum_{n=1}^{L/2} k_n$ with the constraint $0 \leqslant k_1 \leqslant k_2 \cdots \leqslant k_{L/2} \leqslant L/2$. From the number theory we can find the generating function $\Phi(q)$ of $g(K)$, which turns out to be the Gaussian binomial coefficient [37]:

$$\Phi(q) \coloneqq \sum_{K=0}^{L^2/4} g(K) q^K = \binom{L}{L/2}_q \equiv \frac{[L]_q!}{[L - L/2]_q! [L/2]_q!}, \tag{12}$$

where $[L]_q = 1 + q + q^2 + \cdots + q^{L-1}$ is a q-number [37], and $q = \exp(\Delta E/k_B T)$ in this case. By comparing equations (11) and (12) we can find an explicit and exact expression for the partition function of the polymer loop problem:

$$\mathcal{Z}(T) = \Phi(\mathrm{e}^{-\frac{\Delta E}{k_B T}}). \tag{13}$$

Knowing the partition function, we can calculate the occupation probability of each site (see appendix A for details). For large $L \gg 1$ the exact result is almost indistinguishable from the approximation based on the Brownian bridge approach. However, for small L the difference becomes apparent (figure A1 in appendix A). We note that an equivalent result for the generating function of the ASEP with reflecting boundaries was calculated based on $U_q(SU(2))$ quantum group approach in [28].

This section used the mapping of the polymer loop problem to the particle system to explore the statistics of the stationary state. In the next section, we will consider the dynamics of the polymer loop by finding the exact solution to the corresponding ASEP model.

5. Exact solution of ASEP dynamics with reflecting boundaries

We present the exact analytical solution of the ASEP with reflecting boundaries using the Bethe ansatz method [38–40]. The master equation and boundary conditions which define the dynamics of the system as well as further technical details are provided in appendix B. Here we outline the major steps of the solution.

We denote $P(x_1, x_2, \cdots, x_N; t)$ the time dependent probability of finding N particles at coordinates $(x_1, x_2, \cdots, x_N)$ respectively, where $1 \leqslant x_1, x_2, \cdots, x_N \leqslant L$ are integers. To solve the master equation we first use the standard separation of variables ansatz $P(x_1, x_2, \cdots, x_N; t) = \sum_k \Psi_k(x_1, x_2, \cdots, x_N) \mathrm{e}^{\Lambda_k t}$ and aim to find the functions Ψ_k and the corresponding eigenvalues Λ_k. The main idea of the Bethe ansatz method used here is to use the eigenfunctions, which are obtained from a solution for a single-particle hopping on a lattice, as building blocks to construct Ψ_k for the many-particle system (in contrast to using the plane waves of the standard Bethe ansatz previously employed to solve the ASEP model with periodic boundaries [10, 40]). A single-particle solution has two types of eigenfunctions. The first type corresponds to a zero eigenvalue which we refer to as stationary

$$\psi_{\rm s}(x) = Aq^x \tag{14}$$

and the second type corresponding to non-zero eigenvalues which we refer to as non-stationary:

$$\psi_{\rm ns}(x) = q^{\frac{x}{2}}(A_+ {\rm e}^{{\rm i}px} + A_- {\rm e}^{-{\rm i}px}), \tag{15}$$

where $q = \alpha/\beta$ and constants $A, A_\pm$ and p are determined from initial and boundary conditions. We now write down the Bethe ansatz for N particles as:

$$\Psi_k(x_1, x_2, \cdots, x_N) = \sum_{\sigma\in\mathcal{S}_N}\prod_{n=1}^{N}\psi_n^\sigma(x_{\sigma(n)}) \tag{16a}$$

$$\psi_n^\sigma(x) \in \{A^\sigma q^x,\ q^{\frac{x}{2}}(A_+^\sigma {\rm e}^{{\rm i}p_n x} + A_-^\sigma {\rm e}^{-{\rm i}p_n x})\}. \tag{16b}$$

The ansatz is represented as a product of functions $\psi_n^\sigma(x)$ which are chosen in the functional form of the single-particle eigenfunctions. Here $\mathcal{S}_N$ is the group of permutations of N elements. We see that $\Psi(x_1, x_2, \cdots, x_N)$ can have three different compositions. First composition is when all functions $\psi_n^\sigma(x)$ are taken in the stationary form (first term in the curly bracket of equation (16*b*)). Second composition is when all $\psi_n^\sigma(x)$ have a non-stationary form (second term in the curly bracket of equation (16*b*)). The third composition has a mixture of N_s stationary and $N - N_s$ non-stationary $\psi_n^\sigma(x)$.

The case of stationary composition corresponds to the eigenvalue $\Lambda_0 = 0$ and delivers the stationary distribution in agreement with the previously calculated partition function (13) (see appendix A for details) and the result of [28]:

$$P^e(x_1, x_2, \cdots, x_N) = q^{-\frac{N(N+1)}{2}}\binom{L}{N}_q^{-1}\prod_{j=1}^{N} q^{x_j}. \tag{17}$$

When the ansatz Ψ_k, composed solely from non-stationary functions, is substituted into the master equation and boundary conditions are imposed, we obtain the following expression for the eigenvalues:

$$\Lambda_k = \sum_{n=1}^{N}(-(\alpha+\beta) + 2\sqrt{\alpha\beta}\cos(p_n^{\{k\}})). \tag{18}$$

Here $p_n^{\{k\}}$ denotes a kth set of the wave vectors p_n, $n = 1, 2, \ldots N$. These wave-vector sets are obtained as solutions to Bethe equations:

$${\rm e}^{{\rm i}2p_nL} = \prod_{m\neq n}^{N}\frac{a(p_n, p_m)}{a(p_m, p_n)}\frac{a(p_m, -p_n)}{a(-p_n, p_m)}, \tag{19}$$

where $a(p, p') = \sqrt{\alpha\beta}{\rm e}^{{\rm i}(p+p')} - (\alpha+\beta){\rm e}^{{\rm i}p} + \sqrt{\alpha\beta}$. Bethe equations follow from boundary and particle mutual exclusion conditions. We expect to have $C_N^L - C_{N-1}^L$ sets of wave vectors satisfying these nonlinear equations and thus the corresponding number of eigenvalues.

The third composition of the ansatz is a mixture of $N_s < N$ stationary and $N - N_s$ non-stationary functions $\psi_n^\sigma(x)$. It leads to the Bethe equations identical to the case of $N - N_s$ particles, where all $\psi_n^\sigma(x)$ are of non-stationary type. Thus the set of eigenfunctions and eigenvalues of a system with a smaller number of particles is included in that for a system with larger number of particles. For this N has to be smaller than half of the system size, $N \leqslant L/2$, and when it is larger, for symmetry reasons, we can consider vacancies instead of particles. Thus in the regime of mixed ansatz composition we get another $C_{N-1}^L - 1$ eigenvalues and the corresponding eigenfunctions.

The central technical difficulty is to solve the Bethe equation to get the sets of wave vectors and the corresponding set of the eigenvalues. In general, it is a non-trivial task to show that the eigenvalues obtained through the Bethe ansatz approach indeed form a complete set, see for example [41]. We determined the solutions of the Bethe equation numerically and compared the eigenvalues to those obtained by direct diagonalization of the transition matrix in the master equation, see figure 3. In figure 3, we also show that the eigenvalues of the system with a smaller number of particles are always contained in the set of eigenvalues of a system with larger N. Importantly, the subset of eigenvalues corresponding to the single-particle solution can always be calculated explicitly:

$$\Lambda_k = -(\alpha+\beta) + 2\sqrt{\alpha\beta}\cos\left(\frac{k\pi}{L}\right);\ k = 1, 2, \ldots, L-1. \tag{20}$$

Numerical evidence suggests that the single-particle solution provides the smallest (in absolute value) negative eigenvalue ($k = 1$) and thus determines the longest relaxation time

$$\tau = -\frac{1}{\Lambda_1} = \frac{1}{\alpha+\beta-2\sqrt{\alpha\beta}\cos(\pi/L)}. \tag{21}$$

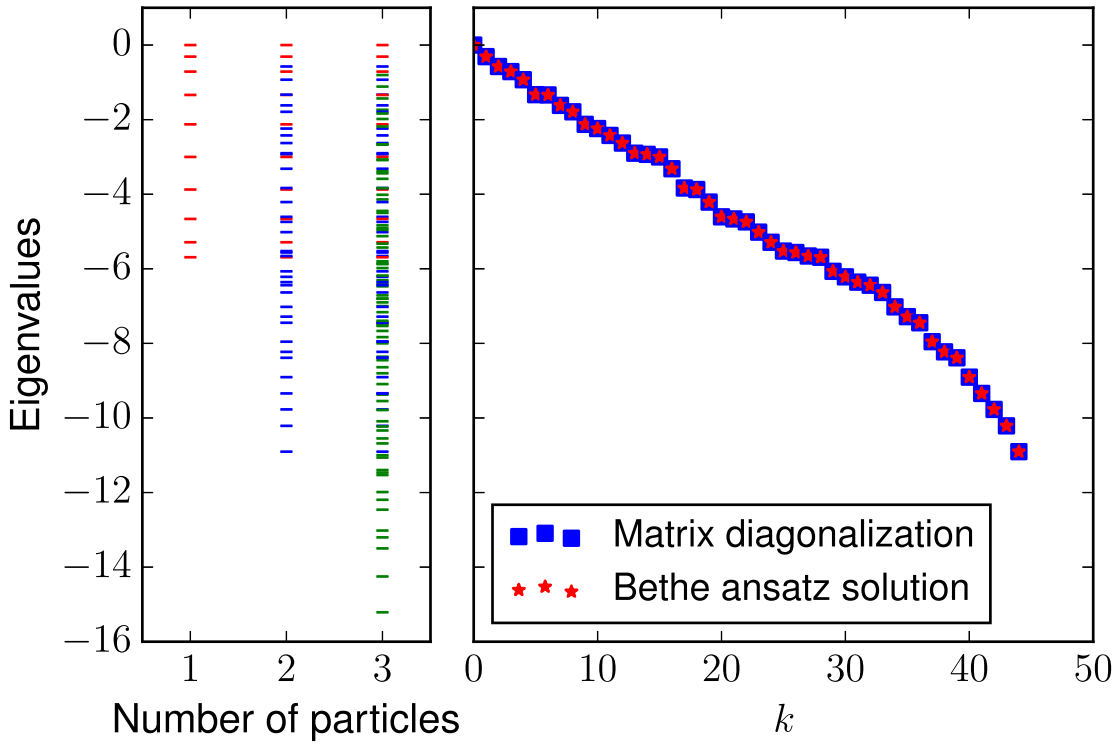

Figure 3. Eigenvalues of the ASEP with reflecting boundaries. The left panel shows eigenvalues of the system of size $L = 10$ with $N = 1, 2$ and 3 particles. The eigenvalues of the system with smaller number of particles are forming a subset in the eigenvalues of the system with larger number of particles, as indicated by colors. The right panel shows eigenvalues obtained from the direct diaganalization of the Markov matrix in the master equation (blue squares) which are compared with those solved from the Bethe equations (red stars). For this figure $\alpha = 2$, $\beta = 1$, $L = 10$ and $N = 2$ for the right panel.

Interestingly, this time does not depend on the particle number N. That means, for example, that for polymer topologies with two ends pinned not at the same but at two different points (which corresponds to N being different from $L/2$) the relaxation times will be the same. Note that an estimate of the relaxation time was also obtained in [28], which is consistent with our exact result equation (21). A very recent manuscript [42] arrived at the same result of equation (21) but in a very different context. The authors of [42] calculated the spectral gap of the Markov chain corresponding to the biased card shuffling problem. They also showed that the time corresponding to this gap is the same as the relaxation time of the ASEP with reflecting boundaries. The method of [42] relies on a discrete version of the Cole-Hopf transform commonly used to solve the nonlinear Burgers equation and allowed the authors to identify the spectral gap.

We now consider an important limiting case of equation (21), when L is large. We can expand the cosine term and get $\tau \simeq 1/((\sqrt{\alpha} - \sqrt{\beta})^2 + \sqrt{\alpha\beta}\pi^2/L^2)$. In the case of no external force ($F = 0$), $\alpha = \beta$ and we arrive at

$$\tau \simeq \tau_{\text{Rouse}} = \frac{L^2}{\sqrt{\alpha\beta}\pi^2} = \frac{L^2\gamma a^2}{k_B T \pi^2}. \tag{22}$$

It is instructive at this point to recall the Rouse relaxation time of the classical bead-spring model, where a polymer is described as a chain of beads connected by harmonic springs [2]. The bead-spring model can be modified to explicitly accommodate the constraint of the pinned loop. It can be shown that it has the same relaxation Rouse time as an unconstrained chain and it is given by equation (22) [43]. By this limiting case we thus validate our choice of the hopping rate r in the particle system. Note the relationship of the relaxation time in the exclusion process to the relaxation time of the Rouse model was also discussed in [44] in the context of reptation model. We should point out that in the limit of the very strong force for a fixed (but large enough) system size L (or in the limit of $L \to \infty$ for a fixed force F) the relaxation time converges to a finite value and is independent of the system size (this can be easily checked by doing the corresponding asymptotic expansion in the exact formula equation (21)). In the picture of a single-particle hopping on a lattice, that could be understood as a situation where at equilibrium the particle is forced to one of the boundaries. Then, either the force is large enough to confine the motion of the particle near to the boundary, or the system size is so large, that the particle behaves effectively as moving on a semi-infinite domain with a single reflecting boundary and thus independent of the actual system size L.

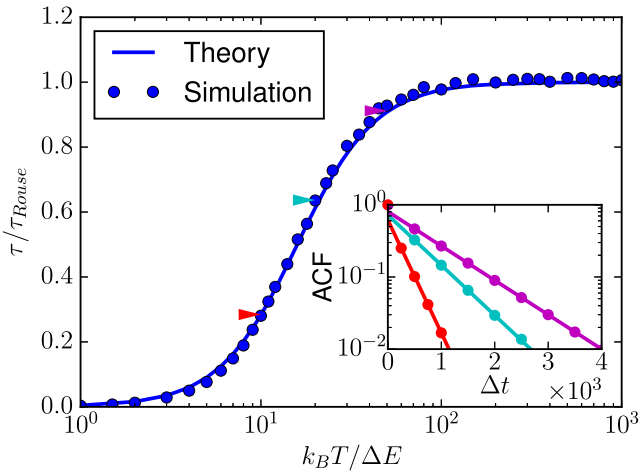

Figure 4. Relaxation time of the ASEP model with reflecting boundaries. The relaxation time is normalized by the Rouse relaxation time equation (22) and plotted as a function of the inverse force expressed by the dimensionless variable $k_BT/\Delta E$, with $\Delta E = 2aF$. Result of the Monte Carlo simulations (dots) are compared with the analytical formula equation (21) (solid line). In the limit of no force $k_BT/\Delta E \to \infty$ the relaxation time of the ASEP saturates to Rouse value. For strong external force $k_BT/\Delta E \to 0$ the relaxation time tends to zero. The inset shows the autocorrelation function (ACF) of the diameter vector as a function of time (colored dots). By fitting an exponential function to the tail of the ACF (colored solid lines) we can extract the corresponding relaxation time. The three values of the relaxation times from the inset are indicated by arrows on the main plot. For this figure $N = 50$, $L = 100$.

To test the analytical results of this section, we numerically investigated the process of relaxation in the one-dimensional pinned polymer loop by performing kinetic Monte Carlo simulations of the corresponding ASEP model. To quantify the relaxation times we computed the time correlation function $\langle z_d(0)z_d(t)\rangle$ of the diameter vector defined by $z_d = z_{L/2} - z_0$. We note that this correlation function was measured for the equilibrated system. Depending on the initial condition, initial dynamics might be different, for example containing periods of ballistic motion if the force was suddenly switched on (for an illustration see supplementary material in [23]). Here, we however, focus on the asymptotic regime of the exponential relaxation. For large times correlations decay exponentially as shown in the inset of figure 4. This allows us to determine the characteristic time of correlations and associate it with the relaxation time of the loop. We see that the relaxation time plotted as a function of the external force matches the analytical results given by the Bethe ansatz, equation (21), see figure 4.

In summary we have demonstrated that the mapping of the one-dimensional polymer model to the ASEP particle system provides solution of the polymer dynamics via the Bethe ansatz approach. However, one may argue that the one-dimensional polymer model is a gross simplification and thus question the relevance of the obtained results for the real polymers. To address this point we compare our results to the relaxation dynamics of a polymer loop in three-dimensions.

6. Relaxation dynamics of a three-dimensional polymer loop

We performed Brownian dynamics simulations of a bead-rod model in three-dimensional space with polymer loop pinned to one point and subject to an external force field (see appendix C for details of numerical simulations). Our focus was on the relaxation dynamics of the polymer loop. By calculating the autocorrelation function of the z-component of the diameter vector $\mathbf{r}_d := \mathbf{r}_{L/2} - \mathbf{r}_0$, we extracted the longest relaxation time of the polymer loop using an exponential fit. We show this relaxation time as a function of the applied force in figure 5. The relaxation time as a function of the applied force shows a behavior very similar to our analytical result obtained in the previous section for the one-dimensional problem. We wondered whether the functional form of equation (21) obtained in one-dimension could be used to describe the results of the three-dimensional simulations. The relaxation time of a polymer loop in three-dimensional space in the absence of an external force can be calculated from the Rouse theory analytically. The one-dimensional result differs from the three-dimensional Rouse time by a simple prefactor of $1/3$ related to the dimensionality of space [2, 4]. Thus the matching prefactor of $1/3$ is also added to the analytical formula equation (21). If we additionally set the energy cost of flipping a bead to $\Delta E = Fa$ (instead of $2Fa$ for one-dimension), the analytical result matches the simulations accurately, as shown in figure 5. Note that there was no fitting involved when comparing theory and numerical data. Thus the one-dimensional model allows us to understand the mechanisms responsible for the relaxation process in the system. It also makes it plausible to suggest that our results can be extended to higher dimensions. Here we should also note that the relaxation dynamics of the diameter vector component

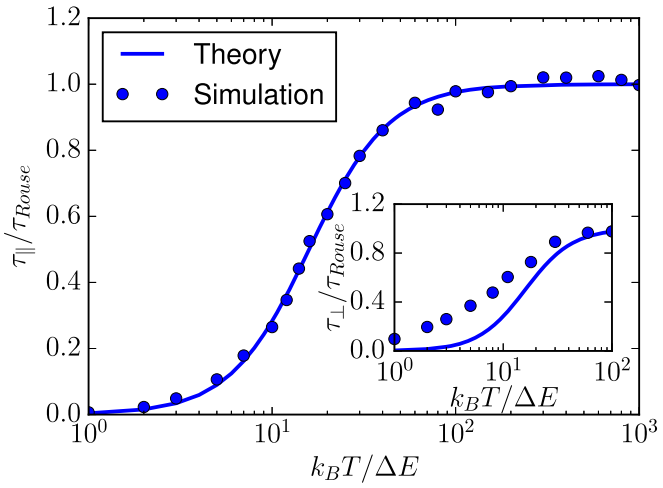

Figure 5. Relaxation time of the three-dimensional pinned polymer loop. We can use the relaxation time of the ASEP model, equation (21), corrected by a factor of $1/3$ to accurately describe the relaxation times of the pinned three-dimensional polymer loop measured in the Brownian dynamics simulations (dots). The main plot shows the relaxation times $\tau_{\parallel}$ of the z-component of the polymer diameter vector $\mathbf{r}_d := \mathbf{r}_{L/2} - \mathbf{r}_0$ as a function of the inverse force expressed in the dimensionless form as $k_BT/\Delta E$ with $\Delta E = Fa$. The inset shows the relaxation time $\tau_{\perp}$ of the diameter vector component perpendicular to the direction of the force from simulations (dots) in comparison the same theoretical prediction of equation (21) (solid line). For this figure the simulated loop consists of $L = 100$ beads.

orthogonal to the direction of the force is clearly distinct from that in the direction of the force (see inset in figure 5).

7. Discussions

We demonstrated that the problem of the pinned one-dimensional polymer loop in an external force field can be mapped to an ASEP on a lattice with reflecting boundaries. While the statistics of the stationary polymer configurations can be asymptotically solved using the Brownian bridge formalism, the ASEP formulation delivers exact solutions for both the steady state distributions and the dynamics. The key technique to solve the ASEP model is the Bethe ansatz method. One of the central results of this analysis is the relaxation time of the polymer loop as a function of applied force and temperature. The relaxation time, which is extracted from the ACF of diameter vector, is decreasing with increasing force. Thus, the external force not only suppresses the fluctuations of the polymer loop but also accelerates the relaxation process. We have shown that the analytical results obtained for the one-dimensional model can be applied to quantify the relaxation dynamics of the three-dimensional polymer loops.

We motivated the model of pulled polymer loops by the biological problem of chromosomal movement in the living cell. Under which assumptions can we expect our equilibrium theory developed for a simple model to be applicable to an intrinsically non-equilibrium and in general more complex biological setting?

(i) Here we neglected the effects of the polymer self-interaction due to the hydrodynamic and excluded volume forces. This allowed us to approximate the effect of the surrounding fluid by a simple Stokes friction resulting in a constant force acting on every bead of the pooled polymer loop. Hydrodynamic interactions are certainly relevant for the low Reynolds number regime of motion in viscous fluids at micro scales. Inclusion of the hydrodynamic interactions in the Zimm model modifies the scaling of the relaxation time of the polymer with its size [5] when compared to the Rouse model. Hydrodynamic interactions are also at the core of the scaling blob theory of polymers by de Genes [1, 45] and its extension to include the effects of the uniform external flow on the pinned polymer [46] and related experiments [47, 48]. To include hydrodynamic interactions in the theoretical framework developed in this paper we would need to make a step from ASEP model to a more general class of stochastic interacting systems [49], which is a very interesting direction of future research.

(ii) Another crucial conceptual simplification is the mapping of the intrinsically non-equilibrium system of the forced polymer dragged through the viscous fluid to an equilibrium problem. The choice of constant pulling speed and not considering the hydrodynamic interactions lead for isotropic beads to a constant average drag force acting on every monomer of the polymer loop. This case can be mapped to an equilibrium problem which can be solved exactly in one-dimension. In a more realistic model, where friction force depends on the local orientation of the polymer or where hydrodynamic interactions play a role, force fluctuations are more complex

and the problem becomes fundamentally a non-equilibrium problem. In particular in the living cell, there are multiple active processes, such as for example activity of molecular motors, chemical reactions, and transcription, which generate additional random forces. To test whether our simplification of a mapping to an equilibrium system provides a good approximation also in non-equilibrium conditions [50–53] is an interesting problem for future studies.

In addition to the particular novel results on polymer dynamics, we would like to highlight the emerging picture of close relationship between very distinct fields of statistical physics discussed in this manuscript. Theory of random walks and Brownian bridges together with Fermi–Dirac statistics are linked to the integer partition number theory. The dynamics of the polymer can be mapped to the ASEP problem with reflecting boundaries. This in turn is related to the card shuffling problem and the discrete version of the Burgers equation [42]. It can be shown [43] that a similar Bethe ansatz method used to solve the ASEP system can be employed for the solution of the single-file diffusion process [54, 55]. In an attempt to extend the study of polymer dynamics beyond one-dimension, multi-species ASEP models can be explored [56–58]. We think that by showing the unification of such apparently different systems and methods used in polymer and statistical physics, we pave the way to their better understanding and ultimately to further new results.

Acknowledgments

We would like to acknowledge stimulating discussions with É Roldán, A Barato, S Majumdar and E Frey. We would like to thank H Spohn for drawing our attention to [42]. Y T Lin was supported by the Center for Nonlinear Studies, Los Alamos National Laboratory and was supported by the Engineering and Physical Sciences Research Council EPSRC (UK) (grant no. EP/K037145/1) when he was affiliated with the School of Physics and Astronomy, The University of Manchester, UK.

Appendix A. Stationary statistics

In the main text, we mention three different ways to get the stationary statistics of the one-dimensional pinned loop. We will compare and benchmark these results here.

The first method is an approximation using the *grand canonical ensemble* and the technique of the Brownian bridge. According to equations (1) and (8*a*), the mean position $\langle z_i \rangle$ of the bead i can be written as

$$\langle z_i \rangle = a\left(2\sum_{j=1}^{i}\mathbb{E}[Z_j] - i\right). \tag{A.1}$$

The variance of the bead position is given by equations (8*b*) and (10). Using equation (7*a*) and converting the summations to integrals when $T \gg 1$, we obtain

$$\langle z_i \rangle = 2a\tilde{T}\ln\left[\frac{1+\exp\left(\frac{L}{2\tilde{T}}\right)}{\exp\left(\frac{\mathrm{i}}{2\tilde{T}}\right)+\exp\left(\frac{L-\mathrm{i}}{2\tilde{T}}\right)}\right], \tag{A.2a}$$

$$\mathrm{var}[z_i] = 2a^2\tilde{T}\frac{\sinh\left(\frac{L-\mathrm{i}}{2\tilde{T}}\right)\sinh\left(\frac{\mathrm{i}}{2\tilde{T}}\right)}{\sinh\left(\frac{L}{2\tilde{T}}\right)\cosh^2\left(\frac{L-2\mathrm{i}}{4\tilde{T}}\right)}, \tag{A.2b}$$

where $\tilde{T} = k_B T/2Fa$.

The second method using *canonical ensemble* and number partition theory and the third method using Bethe ansatz in ASEP both provide the exact solution to the stationary state. We first show the exact partition function obtained from these two methods are equivalent and then compare the exact result to the *Fermi–Dirac* approximation of the first method.

The partition function from the integer partition theory is given in equation (13). According to the generalized Bethe ansatz, the N particles stationary solution of the ASEP system can be constructed as

$$P^e(x_1, x_2, \cdots, x_N) = \Psi_0(x_1, x_2, \cdots, x_N) = A\prod_{j=1}^{N}\left(\frac{\alpha}{\beta}\right)^{x_j}. \tag{A.3}$$

Remembering that $q \equiv \alpha/\beta = \exp(-\Delta E/k_B T)$, one can clearly see the connection between equation (A.3) and the partition function after a variable transformation

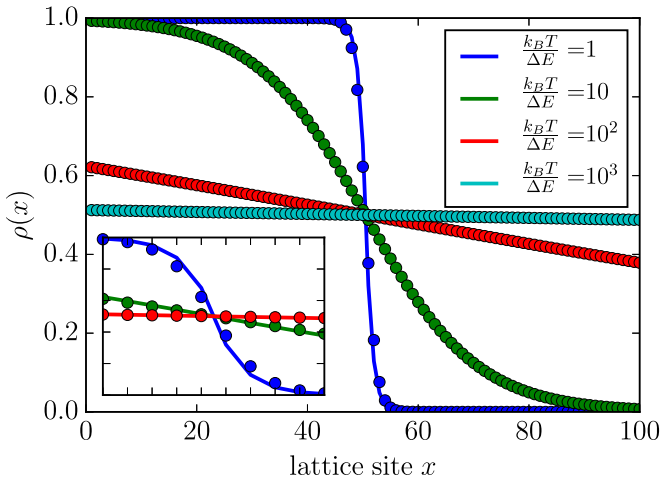

Figure A1. The density profile of the one-dimensional particle system. The Fermi–Dirac approximation (solid lines) is compared with the exact solution of equation (A.8) (symbols). Different cases of hopping bias are illustrated by different colors indicated in the legend. $L = 100$ for the main plot and $L = 10$ for the inset.

$$P^e(x_1, x_2, \cdots, x_N) = A \exp\left(-\frac{E}{k_B T}\right), \tag{A.4}$$

where $E = K\Delta E = (\sum_j x_j - K_0)\Delta E$ with $K_0 = 1 + 2 + \cdots + N = N(N+1)/2$. Thus E is the total energy of the system and K is a integer in the range $0, 1, \cdots, N(L - \mathrm{N})$. Therefore, the partition function is related to the normalization prefactor A:

$$\mathcal{Z}(T) = A^{-1} = \sum_{x_1<x_2<\cdots<x_N} q^{\sum_j x_j} = q^{K_0} \sum_{K=0}^{N(L-N)} g(K) q^K. \tag{A.5}$$

Here $g(K)$, which is identical to $g(E)$, is the number of partitions of a positive integer K into N parts, each of the size of at most $L - N$. From here, we can also identify the Gaussian binomial coefficients

$$\sum_{K=0}^{N(L-N)} g(K) q^K = \binom{L}{N}_q = \frac{[L]_q!}{[L-N]_q![N]_q!}. \tag{A.6}$$

So we finally arrive at equation (17). Meanwhile, by setting $E_0 = K_0\Delta E = 0$ and $N = L/2$ as we did in section 4.3, we obtain exactly the same partition function as equation (13).

With the stationary N particle distribution equation (17), we can readily calculate the equilibrium distribution of any tagged particle. Denoting the distribution of the particle n as $p_n(x)$, we can write

$$\begin{aligned} p_n(x) = & \sum_{0<x_1<\cdots<x_{n-1}\leqslant x-1} P^e(x_1, x_2, \cdots, x_N) \\ & \times \sum_{x<x_{n+1}<\cdots<x_N\leqslant L} P^e(x_1, x_2, \cdots, x_N) \\ = & q^{(N+1-n)(x-n)} \binom{x-1}{n-1}_q \binom{L-x}{N-n}_q \Big/ \binom{L}{N}_q. \end{aligned} \tag{A.7}$$

Finally, the equilibrium density profile, which is the exact counterpart of Fermi–Dirac distribution equation (7), can be obtained by summing up $p_n(x)$

$$\rho(x) = \sum_{n=1}^{N} p_n(x). \tag{A.8}$$

The exact result is shown in figure A1 and compared with the density profile we get from the Fermi–Dirac approximation.

Appendix B. Derivation of the Bethe equations

In this section, we outline the derivation of the Bethe equations presented in the main text. The section is divided into two parts. For illustrative purposes, we consider a single-particle system in the first part. An auxiliary field on a continuous domain will be introduced to solve the discrete master equation. It will be shown that the reflective boundary conditions on the discrete domain can be translated into zero-net-flux conditions for the

auxiliary field on the continuous domain. In the second part, we generalize the analysis for a two-particle system with mutual exclusion. It is shown that the exclusion condition is translated into another zero-net-flux condition for the auxiliary field. We demonstrate that with the Bethe ansatz, the Bethe equation must hold to accommodate all the zero-net-flux conditions. The analysis for the N particle system is a straightforward generalization using the methods presented in this section.

We first consider a single-particle on a lattice $\mathcal{S} := \{1, 2, \ldots L\}$. The particle can hop to its right (if it is not at site L) with a rate α, to its left (if it is not at site 1) with a rate β. For the probability of finding the particle at $j \in \mathcal{S}$ at time t $P_j(t)$, the master equation can be formulated [59, 60]

$$\dot{P}_1(t) = -\alpha P_1(t) + \beta P_2(t), \tag{B.1a}$$

$$\dot{P}_j(t) = -(\alpha + \beta)P_j(t) + \alpha P_{j-1}(t) + \beta P_{j+1}(t),\ 2 \leqslant j \leqslant L - 1, \tag{B.1b}$$

$$\dot{P}_L(t) = -\beta P_L(t) + \alpha P_{L-1}(t). \tag{B.1c}$$

With a specified initial distribution, the above equations (B.1) uniquely describe the evolution of the probability distributions P_j as a function of time t.

The master equation is linear in P_j's and can be succinctly written $\dot{\mathbf{P}} = \mathbf{M} \cdot \mathbf{P}$ where $\mathbf{P}$ is the $n \times 1$ vector $(P_1, \ldots, P_L)$ and $\mathbf{M}$ is the so called Markov matrix. Let $\{\Lambda_k\}_{k=0}^{L-1}$ to be the eigenvalues of $\mathbf{M}$ (in appendix C, we discuss the structure of $\mathbf{M}$ in a general situation of N particles on L lattice sites). The case when $\Lambda_0 = 0$ corresponds to the stationary distribution of the system considered in the previous appendix A. In the following, we focus on the case of non-stationary solution when $\Lambda_k \neq 0$.

Now we introduce an auxiliary field $R(x, t)$ on a domain $x \in \mathbb{R}$ and $t \in \mathbb{R}^+$. The idea is to impose $P_j(t) \equiv R(j, t)$, so that the evolution equations (B.1) are transformed into difference equations for the field $R(x, t)$. By separation of variables, we first write

$$R(x, t) = \sum_k \psi_k(x)\exp(\Lambda_k t). \tag{B.2}$$

By plugging equation (B.2) into (B.1), we arrive at the following equations for ψ_k evaluated on $x \in \mathcal{S}$:

$$\Lambda_k\psi_k(1) = -\alpha\psi_k(1) + \beta\psi_k(2), \tag{B.3a}$$

$$\Lambda_k\psi_k(j) = -(\alpha + \beta)\psi_k(j) + \alpha\psi_k(j - 1) + \beta\psi_k(j + 1),\ 2 \leqslant j \leqslant L - 1, \tag{B.3b}$$

$$\Lambda_k\psi_k(L) = -\beta\psi_k(L) + \alpha\psi_k(L - 1). \tag{B.3c}$$

Note that equation (B.3) are only imposed on the lattice sites $x \in \mathcal{S}$. Next, we extend equation (B.3) to $x \in \mathbb{R}$ by demanding

$$\Lambda_k\psi_k(x) = -(\alpha + \beta)\psi_k(x) + \alpha\psi_k(x - 1) + \beta\psi_k(x + 1),\ \forall x \in \mathbb{R}. \tag{B.4}$$

The extended equation (B.4) is consistent with the evolution equation for the discrete probabilities on the interior lattice sites (equation (B.3*b*)). The boundary equations on the discrete domain, (B.3*a*) and (B.3*c*), can also be satisfied by imposing a zero flux condition for the auxiliary field ψ_k:

$$0 = \alpha\psi_k(0) - \beta\psi_k(1), \tag{B.5a}$$

$$0 = \alpha\psi_k(L) - \beta\psi_k(L + 1). \tag{B.5b}$$

It can be shown that the solution of equation (B.4) with the zero-net-flux conditions (B.5) evaluated on the discrete lattice site $\mathcal{S}$ solves the original equation (B.3), using the transformation $P_j(t) = \sum_k \psi_k(j)\exp(\Lambda_k t)$.

The boundary conditions (B.5) can be interpreted in the following way. While the discrete dynamics (B.1) does not take place outside of the domain $\mathcal{S}$, by extending the domain to a continuous real x, the reflecting boundary conditions on the discrete domain are preserved under zero-net-flux conditions at the boundaries of the continuous domain. For example, equation (B.5) imposes a condition such that the flux from $x = 0$ to $x = 1$ (which is $\alpha P_0(t) \propto \alpha\psi(0)$) equals to the flux from $x = 1$ to $x = 0$ (which is $\beta P_1(t) \propto \beta\psi(1)$). This construction is in the same spirit as the introduction of the 'ghost points' when using finite difference methods to solve differential equations with reflecting boundaries.

We remark that in the original discrete process both P_0 and P_{L+1} should be 0: the probabilities of finding a particle outside the domain are zero. The fluxes from P_1 to P_0 and P_L to P_{L+1} are also zero: it is forbidden for the particle to jump outside of the domain. The boundary conditions (B.5) are only meaningful on the auxiliary field ψ which has a continuous domain $x \in \mathbb{R}$, and on this domain $\psi(x < 1)$ and $\psi(x > L)$ are not zero in general.

To solve equation (B.4), the standard ansatz is

$$\psi(x) = C_+ z_+^x + C_- z_-^x, \tag{B.6}$$

where z_+, z_- are two complex roots of the characteristic equation $\beta z^2 - (\alpha + \beta + \Lambda)z + \alpha = 0$ and C_+, C_- are two unfixed coefficients. After plugging the equation (B.6) in the reflecting boundary condition (B.5), we find L eigenvalues Λ and the corresponding $\psi(x)$. For $\Lambda_0 = 0$, the corresponding $\psi(x)$ is stationary and $\psi_s(x)$ can be written in the form of equation (14). The $L-1$ non-stationary eigenvalues correspond to $\psi_{ns}(x)$ in the form of equation (15) and can be calculated as $\Lambda_k = -\alpha - \beta + 2\sqrt{\alpha\beta}\cos(k\pi/L)$, $k = 1, 2, \ldots, L-1$. It is possible to fix all coefficients of $\psi_s(x)$ and $\psi_{ns}(x)$ using the normalization and boundary conditions. However, we keep them for the convenience of the following calculations.

Next, we move on to the two-particle case. Denote the probability of finding the first particle at i and the second at j at time t by $_{Pi,\,j}(t)$. We shall preserve the order $1 \leqslant i < j \leqslant L$. The explicit form of the evolution equations depends on (1) if the particles are right next to each other and (2) if one of the particles is at the boundary sites ($i = 1$ or $i = L$). As the number of particles in the system increases, explicitly expressing the evolution equations for the system becomes impractical because of the mutual exclusion condition. Nevertheless, we can still extend the evolution equation to a continuous domain $(x_1, x_2) \in \mathbb{R}^2$. We write an auxiliary field $R(x_1, x_2, t) = \sum_k \Psi_k(x_1, x_2)\exp(\Lambda_k t)$, and the evolution equation (without reflecting boundary conditions and exclusive condition) suggests the following difference equation on this auxiliary function

$$\begin{aligned}\Psi_k(x_1, x_2) = &-2(\alpha + \beta)\Psi_k(x_1, x_2)\\ &+ \alpha\Psi_k(x_1 - 1, x_2) + \alpha\Psi_k(x_1, x_2 - 1)\\ &+ \beta\Psi_k(x_1 + 1, x_2) + \beta\Psi_k(x_1, x_2 + 1).\end{aligned} \tag{B.7}$$

The reflective boundary conditions on the discrete domain are translated into zero-net-flux conditions at $x_1 = 0$ and $x_2 = L$:

$$0 = \alpha\Psi_k(0, x_2) - \beta\Psi_k(1, x_2), \tag{B.8a}$$

$$0 = \alpha\Psi_k(x_1, L) - \beta\Psi_k(x_1, L + 1). \tag{B.8b}$$

The mutual exclusion condition can be imposed by demanding zero-net-flux to and out of the set $\Psi_k(x, x)$:

$$(\alpha + \beta)\Psi_k(x, x + 1) = \alpha\Psi_k(x, x) + \beta\Psi_k(x + 1, x + 1) \tag{B.9}$$

for all $x \in \mathbb{R}$. This equation can be interpreted as follows: when two particles sit next to each other at $(x, x + 1)$, the potential right-hopping of the left particle and the left-hopping of the right particle are forbidden by the exclusiveness. In the generalized evolution equation (B.7) this possibility is not forbidden but instead, the zero-net-flux boundary condition (B.9) is imposed. We again emphasize that $\Psi(0, x_2)$, $\Psi(x_1, L + 1)$, and $\Psi(x, x)$ are the values of the auxiliary field evaluated on the extended domain, and are generally not zero while the physical probabilities $P_{0,i} = P_{i,L+1} = P_{i,i} = 0$ for $i \in \mathcal{S}$.

Equations (B.7), (B.8), and (B.9) uniquely determine the auxiliary field $\Psi(x_1, x_2)$. Bethe ansatz postulates

$$\Psi(x_1, x_2) = \psi_1(x_1)\psi_2(x_2) + \tilde{\psi}_1(x_2)\tilde{\psi}_2(x_1), \tag{B.10}$$

where ψ_1 and ψ_2 (similarly, $\tilde{\psi}_1$ and $\tilde{\psi}_2$) belong to the same 'type' of single-particle solution (either both stationary solutions or both non-stationary solutions) having the same momentum p. If the non-stationary ansatz is chosen, the momenta p_1 and p_2 need to be found by imposing the boundary conditions of the two-particle case; they are not in general the solutions of the single-particle model.

It can be shown that the ansatz (B.10) solves the evolutionary equation (B.7). Depending on the selection of the types of ψ_i and $\tilde{\psi}_i$, the resulting equations after imposing the boundary conditions (B.8) and (B.9) are different. For illustrative purpose, we present the analysis for the case when all the ψ_i and $\tilde{\psi}_i$ are chosen in a non-stationary form:

$$\psi_{\{1,2\}}(x) \coloneqq A_{\{1,2\}+}e^{ip_{\{1,2\}}x} + A_{\{1,2\}-}e^{-ip_{\{1,2\}}x}, \tag{B.11a}$$

$$\tilde{\psi}_{\{1,2\}}(x) \coloneqq \tilde{A}_{\{1,2\}+}e^{ip_{\{1,2\}}x} + \tilde{A}_{\{1,2\}-}e^{-ip_{\{1,2\}}x}. \tag{B.11b}$$

Plug the ansatz (B.10) into the reflective boundary conditions (B.8) and after some algebra, we arrive at

$$\frac{A_{1+}}{A_{1-}} = -\frac{\sqrt{\alpha} - \sqrt{\beta}e^{-ip_1}}{\sqrt{\alpha} - \sqrt{\beta}e^{ip_1}}, \quad \frac{\tilde{A}_{1+}}{\tilde{A}_{1-}} = \frac{A_{1+}}{A_{1-}}e^{-2ip_1L}, \tag{B.12}$$

$$\frac{\tilde{A}_{2+}}{\tilde{A}_{2-}} = -\frac{\sqrt{\alpha} - \sqrt{\beta}e^{-ip_2}}{\sqrt{\alpha} - \sqrt{\beta}e^{ip_2}}, \quad \frac{A_{2+}}{A_{2-}} = \frac{\tilde{A}_{2+}}{\tilde{A}_{2-}}e^{-2p_2L}. \tag{B.13}$$

At the same time the mutual exclusion condition equation (B.9) results in

$$\frac{A_{1+}A_{2+}}{\tilde{A}_{1+}\tilde{A}_{2+}} = -\frac{a(p_1, p_2)}{a(p_2, p_1)}, \frac{A_{1+}A_{2-}}{\tilde{A}_{1+}\tilde{A}_{2-}} = -\frac{a(p_1, -p_2)}{a(-p_2, p_1)}$$
$$\frac{A_{1-}A_{2+}}{\tilde{A}_{1-}\tilde{A}_{2+}} = -\frac{a(-p_1, p_2)}{a(p_2, -p_1)}, \frac{A_{1-}A_{2-}}{\tilde{A}_{1-}\tilde{A}_{2-}} = -\frac{a(-p_1, -p_2)}{a(-p_2, -p_1)}, \tag{B.14}$$

where $a(p, p') \coloneqq \sqrt{\alpha\beta}\mathrm{e}^{\mathrm{i}(p+p')} - (\alpha + \beta)\mathrm{e}^{\mathrm{i}p} + \sqrt{\alpha\beta}$. Using the identities

$$\left(\frac{A_{1+}}{A_{1-}}\right)\left(\frac{\tilde{A}_{1-}}{\tilde{A}_{1+}}\right) = \left(\frac{A_{1+}A_{2+}}{\tilde{A}_{1+}\tilde{A}_{2+}}\right)\left(\frac{\tilde{A}_{2+}\tilde{A}_{1-}}{A_{2+}A_{1-}}\right) \tag{B.15a}$$

$$\left(\frac{\tilde{A}_{2+}}{\tilde{A}_{2-}}\right)\left(\frac{A_{2-}}{A_{2+}}\right) = \left(\frac{\tilde{A}_{1+}\tilde{A}_{2+}}{A_{1+}A_{2+}}\right)\left(\frac{A_{1+}A_{2-}}{\tilde{A}_{1+}\tilde{A}_{2-}}\right) \tag{B.15b}$$

we arrive at the Bethe equation presented in the main text:

$$\mathrm{e}^{\mathrm{i}2p_1L} = \frac{a(p_1, p_2)}{a(p_2, p_1)}\frac{a(p_2, -p_1)}{a(-p_1, p_2)} \tag{B.16a}$$

$$\mathrm{e}^{\mathrm{i}2p_2L} = \frac{a(p_2, p_1)}{a(p_1, p_2)}\frac{a(p_1, -p_2)}{a(-p_2, p_1)}. \tag{B.16b}$$

A similar analysis shows that if one of the ψ, $\tilde{\psi}$ pairs is stationary and the other is non-stationary, the boundary conditions (B.8) and (B.9) recover the single-particle case

$$\mathrm{e}^{\mathrm{i}2pL} = 1. \tag{B.17}$$

Appendix C. Simulation methods

Extensive simulations, including the Monte Carlo simulation of the ASEP and Brownian dynamics simulation of the 3D pinned polymer loop, were carried out to test theoretical predictions. ASEP is a continuous time Markov chain, so the standard kinetic Monte Carlo algorithm [61] is employed to generate exact sample paths for numerical calculation of the statistical quantities. To perform matrix diagonalization in figure 3, we first need to construct the many-particle transition matrix $\mathbf{M}$. The dimension of $\mathbf{M}$ is $C_N^L \times C_N^L$. The matrix $\mathbf{M}$ is constructed by enumerating all possible many-particle configurations $\{\eta\}$ of the ASEP. The transition rate $M_{\eta,\eta'}$ is set to α if a configuration η can be reached from another configuration $\eta' \neq \eta$ by an event of a single-particle hopping to the right. Similarly, $M_{\eta',\eta} = \beta$. The diagonal elements are prescribed by conservation of probabilities, $M_{\eta,\eta} = -\sum_{\eta'\neq\eta} M_{\eta',\eta}$. The eigenvalues of $\mathbf{M}$ are obtained by standard numerical matrix diaganalization methods [62].

The details of the Brownian dynamics simulation are discussed below. We adopted a simple freely jointed bead-rod model, where the beads are connected by massless rigid rods. In an overdamped regime, the inertia of the beads can be neglected. Consequently, the evolution equation for each bead is

$$\gamma\frac{\mathrm{d}\mathbf{r}_i}{\mathrm{d}t} = \mathbf{F}_i^c + \mathbf{F}_i^e + \mathbf{F}_i^b + \mathbf{F}_i^{\mathrm{pseudo}}, \tag{C.1}$$

where γ is the friction coefficient, $\mathbf{F}_i^c$ is the constraint force which keeps the rod at constant length, $\mathbf{F}_i^e$ is the external force (drag exerted by the fluid), $\mathbf{F}_i^b$ is the multi-variate Brownian force whose statistics satisfy $\langle \mathbf{F}_i^b \rangle = \mathbf{0}$ and $\langle f_{im}^b(t) f_{jn}^b(t') \rangle = 2\gamma k_B T \delta_{ij}\delta_{mn}\delta(t - t')$, and $\mathbf{F}_i^{\mathrm{pseudo}}$ is the pseudo force added to preserve the correct statistics of the constrained system: $\mathbf{F}_i^{\mathrm{pseudo}} = -\partial U_{\mathrm{met}}/\partial \mathbf{r}_i$; $U_{\mathrm{met}} \coloneqq k_B T \ln(\det \mathbf{G})/2$, and $\mathbf{G}$ is the metric tensor [63].

Using the predictor-corrector algorithm, each of the the constraint forces $\{\mathbf{F}_i^c\}_{i=1}^L$ is calculated implicitly by solving the constraint equation $|\mathbf{r}_{i+1} - \mathbf{r}_i| = a$. In order to pin the polymer loop in space, we add a 'phantom' rod with zero length at the pinned bead at the origin.

ORCID iDs

Wenwen Huang https://orcid.org/0000-0002-3857-0143
Yen Ting Lin https://orcid.org/0000-0001-6893-8423
Jaeoh Shin https://orcid.org/0000-0002-2365-5793
Frank Jülicher https://orcid.org/0000-0003-4731-9185

References

[1] De Gennes P G 1979 *Scaling Concepts in Polymer Physics* (New York: Cornell University Press)
[2] Doi M and Edwards S F 1988 *The Theory of Polymer Dynamics* (Oxford: Oxford University Press)
[3] Jun S and Wright A 2010 Entropy as the driver of chromosome segregation *Nat. Rev. Microbiol.* **8** 600–7
[4] Rouse P E 1953 A theory of the linear viscoelastic properties of dilute solutions of coiling polymers *J. Chem. Phys.* **21** 1272–80
[5] Zimm B H 1956 Dynamics of polymer molecules in dilute solution: viscoelasticity, flow birefringence and dielectric loss *J. Chem. Phys.* **24** 269–78
[6] Fritsche M and Heermann D W 2011 Confinement driven spatial organization of semiflexible ring polymers: implications for biopolymer packaging *Soft Matter* **7** 6906–13
[7] Perkins T, Smith D, Larson R and Chu S 1995 Stretching of a single tethered polymer in a uniform flow *Science* **268** 83–7
[8] Mohan A and Doyle P S 2007 Unraveling of a tethered polymer chain in uniform solvent flow *Macromolecules* **40** 4301–12
[9] Lang P S, Obermayer B and Frey E 2014 Dynamics of a semiflexible polymer or polymer ring in shear flow *Phys. Rev.* E **89** 022606
[10] Derrida B 1998 An exactly soluble non-equilibrium system: the asymmetric simple exclusion process *Phys. Rep.* **301** 65–83
[11] Bressloff P C and Newby J M 2013 Stochastic models of intracellular transport *Rev. Mod. Phys.* **85** 135–96
[12] Schütz G 2001 *Exactly Solvable Models for Many-Body Systems Far from Equilibrium* (New York: Academic)
[13] Panyukov S and Rabin Y 2001 Fluctuating elastic rings: statics and dynamics *Phys. Rev.* E **64** 011909
[14] Sakaue T 2011 Ring polymers in melts and solutions: scaling and crossover *Phys. Rev. Lett.* **106** 167802
[15] Kim J, Yang Y and Lee W 2012 Self-consistent field theory of gaussian ring polymers *Macromolecules* **45** 3263–9
[16] McLeish T 2002 Polymers without beginning or end *Science* **297** 2005–6
[17] Alim K and Frey E 2007 Shapes of semiflexible polymer rings *Phys. Rev. Lett.* **99** 198102
[18] Robertson R M and Smith D E 2007 Strong effects of molecular topology on diffusion of entangled DNA molecules *Proc. Natl Acad. Sci. USA* **104** 4824–7
[19] Reith D, Mirny L and Virnau P 2011 GPU based molecular dynamics simulations of polymer rings in concentrated solution: structure and scaling *Prog. Theor. Phys. Suppl.* **191** 135–45
[20] Haarhuis J *et al* 2017 The cohesin release factor WAPL restricts chromatin loop extension *Cell* **169** 693–707
[21] Dekker J and Mirny L 2016 The 3D genome as moderator of chromosomal communication *Cell* **164** 1110–21
[22] Goloborodko A, Imakaev M V, Marko J F and Mirny L 2016 Compaction and segregation of sister chromatids via active loop extrusion *eLife* **5** e14864
[23] Lin Y T *et al* 2015 Pulled polymer loops as a model for the alignment of meiotic chromosomes *Phys. Rev. Lett.* **115** 208102
[24] Vogel S K, Pavin N, Maghelli N, Jülicher F and Tolić I M 2009 Self-organization of dynein motors generates meiotic nuclear oscillations *PLoS Biol.* **7** e1000087
[25] Chacón M R, Petrina D and Tolić I M 2016 Meiotic nuclear oscillations are necessary to avoid excessive chromosome associations *Cell Rep.* **17** 1632–45
[26] Hänggi P, Talkner P and Borkovec M 1990 Reaction-rate theory: 50 years after Kramers *Rev. Mod. Phys.* **62** 251–341
[27] Katz S, Lebowitz J L and Spohn H 1983 Phase transitions in stationary non-equilibrium states of model lattice systems *Phys. Rev.* B **28** 1655–8
[28] Sandow S and Schütz G 1994 On $U_q[SU(2)]$-symmetric driven diffusion *Europhys. Lett.* **26** 7–12
[29] Lawler G F and Limic V 2010 *Random Walk: A Modern Introduction* (Cambridge: Cambridge University Press)
[30] Comtet A, Leboeuf P and Majumdar S N 2007 Level density of a Bose gas and extreme value statistics *Phys. Rev. Lett.* **98** 070404
[31] Majumdar S N, Randon-Furling J, Kearney M J and Yor M 2008 On the time to reach maximum for a variety of constrained Brownian motions *J. Phys. A: Math. Theor.* **41** 365005
[32] Majumdar S N and Orland H 2015 Effective Langevin equations for constrained stochastic processes *J. Stat. Mech.* P06039
[33] Chandler D 1987 *Introduction to Modern Statistical Mechanics* (Oxford: Oxford University Press)
[34] Huang K 1987 *Statistical Mechanics* (New York: Wiley)
[35] Feller W 2008 *An Introduction to Probability Theory and Its Applications* (New Delhi: Wiley India Pvt. Limited)
[36] Athreya K B and Lahiri S N 2006 *Measure Theory and Probability Theory* (New York: Springer)
[37] Andrews G E 1998 *The Theory of Partitions* (Cambridge: Cambridge University Press)
[38] Simon D 2009 Construction of a coordinate Bethe ansatz for the asymmetric simple exclusion process with open boundaries *J. Stat. Mech.* P007017
[39] Batchelor M T 2007 The Bethe ansatz after 75 years *Phys. Today* **60** 36–40
[40] Mallick K 2011 Some exact results for the exclusion process *J. Stat. Mech.* P01024
[41] Brattain E, Do N and Saenz A 2015 The completeness of the Bethe ansatz for the periodic ASEP arXiv:1511.03762
[42] Labbé C and Lacoin H 2016 Cutoff phenomenon for the asymmetric simple exclusion process and the biased card shuffling arXiv:1610.07383
[43] Huang W 2018 *PhD Thesis* TU Dresden
[44] Schütz G 1999 Non-equilibrium relaxation law for entangled polymers *Europhys. Lett.* **48** 623–8
[45] Pincus P 1976 Excluded volume effects and stretched polymer chains *Macromolecules* **9** 386–8
[46] Brochard-Wyart F 1995 Polymer chains under strong flows: stems and flowers *Europhys. Lett.* **30** 387–92
[47] Manneville S, Cluzel P, Viovy J, Chatenay D and Caron F 1996 Evidence for the universal scaling behaviour of a freely relaxing DNA molecule *Europhys. Lett.* **36** 413–8
[48] Perkins T, Quake S, Smith D and Chu S 1994 Relaxation of a single DNA molecule observed by optical microscopy *Science* **264** 822–6
[49] Liggett T M 2005 *Interacting Particle Systems* (Berlin: Springer)
[50] Battle C *et al* 2016 Broken detailed balance at mesoscopic scales in active biological systems *Science* **352** 604–7
[51] Prost J, Jülicher F and Joanny J F 2015 Active gel physics *Nat. Phys.* **11** 111–7
[52] Mestres P, Martinez I A, Ortiz-Ambriz A, Rica R A and Roldan E 2014 Realization of nonequilibrium thermodynamic processes using external colored noise *Phys. Rev.* E **90** 032116
[53] Marchetti M C *et al* 2013 Hydrodynamics of soft active matter *Rev. Mod. Phys.* **85** 1143–89
[54] Lizana L and Ambjörnsson T 2008 Single-file diffusion in a box *Phys. Rev. Lett.* **100** 200601
[55] Barkai E and Silbey R 2009 Theory of single file diffusion in a force field *Phys. Rev. Lett.* **102** 050602
[56] Schütz G and Wehefritz-Kaufmann B 2017 Kardar-Parisi-Zhang modes in d-dimensional directed polymers *Phys. Rev.* E **96** 032119
[57] Finn C, Ragoucy E and Vanicat M 2018 Matrix product solution to multi-species ASEP with open boundaries *J. Stat. Mech.* 043201
[58] Arita C and Mallick K 2013 Matrix product solution to an inhomogeneous multi-species TASEP *J. Phys. A: Math. Theor.* **46** 085002

[59] Van Kampen N G 2007 *Stochastic Processes in Physics and Chemistry* (Amsterdam: Elsevier)
[60] Gardiner C W 2004 *Handbook of Stochastic Methods* (Berlin: Springer)
[61] Gillespie D T 1976 A general method for numerically simulating the stochastic time evolution of coupled chemical reactions *J. Comput. Phys.* **22** 403–34
[62] Press W H 2007 *Numerical Recipes: The Art of Scientific Computing* (Cambridge: Cambridge University Press)
[63] Pasquali M and Morse D C 2002 An efficient algorithm for metric correction forces in simulations of linear polymers with constrained bond lengths *J. Chem. Phys.* **116** 1834–8